Macromolecular Rapid Communications
www.mrc-journal.de

4D Printed Actuators with Soft-Robotic Functions

*María López-Valdeolivas, Danqing Liu, Dick Jan Broer, and Carlos Sánchez-Somolinos**

Soft matter elements undergoing programed, reversible shape change can contribute to fundamental advance in areas such as optics, medicine, microfluidics, and robotics. Crosslinked liquid crystalline polymers have demonstrated huge potential to implement soft responsive elements; however, the complexity and size of the actuators are limited by the current dominant thin-film geometry processing toolbox. Using 3D printing, stimuli-responsive liquid crystalline elastomeric structures are created here. The printing process prescribes a reversible shape-morphing behavior, offering a new paradigm for active polymer system preparation. The additive character of this technology also leads to unprecedented geometries, complex functions, and sizes beyond those of typical thin-films. The fundamental concepts and devices presented therefore overcome the current limitations of actuation energy available from thin-films, thereby narrowing the gap between materials and practical applications.

1. Introduction

Soft material structures that reversibly change their shape in a programed fashion in response to an external stimulus are essential elements to implement new actuators and smart devices of application in medicine,[1] microfluidics,[2] adaptive optics,[3] haptics,[4] and robotics.[5] Materials employed include elastomers actuated by pneumatic or hydraulic means,[6] electroactive polymers,[7] as well as patterned hydrogels that shape-shift on swelling.[8,9] Further development of soft elements capable to perform complex motions or functions requires adequate materials and processing technologies that enable accurate control of the mechanical response. Moreover, on the route toward practical applications, there is often a necessity to have the possibility to miniaturize these elements, produce them in large dimensions or over large areas, or integrate them with other materials, elements, or devices.

Crosslinked liquid crystalline polymers (LCPs) have received much attention as candidates for this purpose since they can exhibit large macroscopic scale mechanical response to different external stimuli such as heat, light, pH, or moisture.[10–12] Thin-films of these materials with controlled molecular orientation, defined by the director (*n*), have predominantly been investigated as building blocks to implement a variety of responsive elements or devices.[13–22] However the thin-film character of these elements markedly limits the energy available for actuation. Even more, the reported systems, including their processing toolbox, are limited to one single material and therefore multifunctional and multiresponsive systems are difficult to create. For the true development and incorporation of these LCP structures in real life applications, the capability to generate elements of different sizes, from very small to very large, is fundamental. This needs to be done with a precise control of the material morphology and properties as well as director orientation in well-defined complex geometries, all together leading to an accurate control of the mechanical response.

Additive manufacturing techniques enable digital generation of material patterns in surfaces or fabrication of 3D objects. While 3D printing of conventional materials leads to inanimate 3D objects with static shape, 4D printing of responsive materials adds a 4th dimension as it leads to architectures that, with an appropriate stimulus, change their shape over time.[9,23] Here, we report the 4D printing of liquid crystalline elastomer (LCE) macro- and microstructures. Digital control of the local anisotropy of the applied LC material is advantageously achieved through the printing process. This allows to precisely program the magnitude and directionality of the forces in response to the external stimulus, temperature in our case, and therefore well-defined reversible shape-morphing of the structures in space and time. Although 4D printing has been recently described with hydrogels charged with anisotropic cellulose fibrils that get oriented during printing,[9] the mechanical response of these materials is based on water swelling, which limits the applicability due to the specific and stringent environment required for actuation as well as the slow response

M. López-Valdeolivas, Dr. C. Sánchez-Somolinos
Departamento de Física de la Materia Condensada
Instituto de Ciencia de Materiales de Aragón (ICMA)
CSIC-Universidad de Zaragoza, Zaragoza 50009, Spain
E-mail: carlos.s@csic.es
Dr. D. Liu, Prof. D. J. Broer
Laboratory of Functional Organic Materials and Devices
Department of Chemical Engineering and Chemistry
Eindhoven University of Technology
P.O. Box 513, 5600 MB Eindhoven, The Netherlands
Dr. D. Liu, Prof. D. J. Broer
Institute for Complex Molecular Systems
Eindhoven University of Technology
5600 MB, Eindhoven, The Netherlands
Dr. C. Sánchez-Somolinos
CIBER in Bioengineering
Biomaterials and Nanomedicine (CIBER-BBN), Zaragoza 50018, Spain
The ORCID identification number(s) for the author(s) of this article can be found under https://doi.org/10.1002/marc.201700710.

DOI: 10.1002/marc.201700710

time in the range of several minutes. In contrast to this, LCPs can be precisely tailored to be reversibly responsive to a wide variety of stimuli, other than moisture, although this is not excluded, and to respond in shorter times overcoming these limitations.[11] Complex geometries, difficult to achieve with the currently available processing technologies for LCPs, are easily implemented using our 4D printing platform, bringing also new shape-morphing possibilities and therefore functions to the liquid crystal actuator arena. By stacking two or more layers of 3D printed material, the resulting assemblies overcome one of the current principle shortcomings of LCP thin-film technology, which is the limited amount of energy available for actuation in thin-films, thereby broadening the scope of these materials toward, for example, complex artificial muscles with high work capacity.

2. Results and Discussion

2.1. 4D Printing Platform

Our ink is a mixture of a reactive main-chain LCP bearing reactive acrylate groups at the chain ends and a photoinitiator (**Figure 1**a). The reactive polymer is obtained by addition of a LC diacrylate to *n*-butylamine.[21,24] The ink shows viscoelastic behavior at room temperature (RT), enabling easy formation of long fibers just by manually drawing them from the polymer with tweezers. The substoichiometric amount of amine used favors that the synthesized polymer chains retain acrylate functionalities at their ends. The reactive groups can subsequently react in a second stage by ultraviolet (UV) initiated free-radical polymerization.

Ink printing is carried out using an extrusion-based 3D printer, consisting of a computer numerical control (CNC) router coupled to a fluid dispenser. Figure 1b shows a schematic view of the manufacturing process: After extrusion and deposition, the resulting printed lines can be subsequently fixed by UV photoexposure. This triggers the polymerization of the acrylate end-groups, leading to a crosslinked elastomer. During extrusion and deposition, shear forces and/or elongational flow are expected to favor the polymer chain alignment, building up orientational order of the mesogens along the needle moving direction (Figure 1c).

Figure 1d,e shows polarization optical microscope (POM) images of a line of material printed on top of a glass substrate, respectively, at 0° and 45° to the first polarizer transmission direction. These POM images together with printing experiments using ink containing a dichroic dye (Figure S1, Supporting Information) indicate director alignment along the printing direction. After photopolymerization, the line presents the same anisotropic characteristics as the uncured sample, even if photoexposure is carried out minutes after deposition. The printing process can be repeated layer by layer as illustrated in Figure 1b.

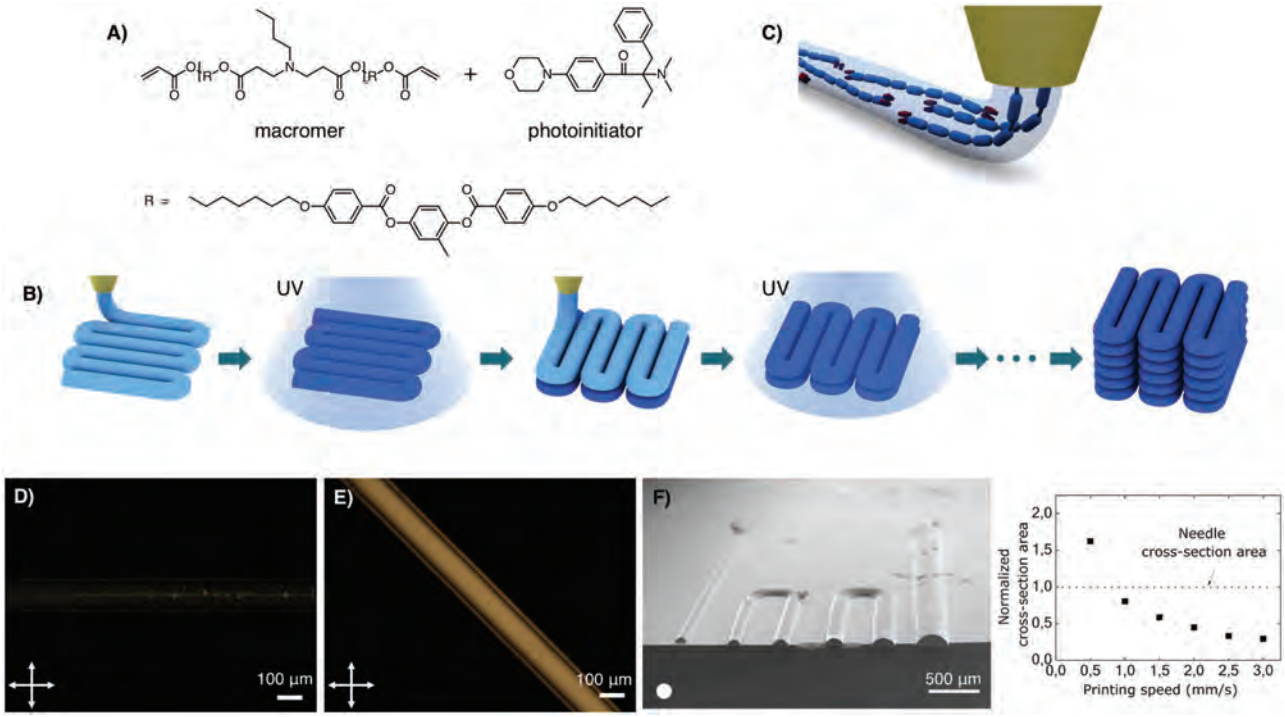

Figure 1. 4D printing of LCEs. a) Ink components molecular structure. b) Printing process schematic description: Ink, digitally deposited to create a structured layer, is subsequently photopolymerized. Successive layers can be added by stepwise printing and curing material on top. c) Conceptual representation of the imposed polymer main-chain alignment along the printing direction. Printed polymer lines between crossed polarizers (crosses indicate polarization directions) with the line direction oriented d) parallel and e) at 45° with respect to the first polarizer transmission direction. f) Cross-sectional SEM images of freeze-fractured lines printed with different needle displacement speeds (from left to right: 3, 2.5, 2, 1.5, 1, 0.5 mm s^{-1}). A white circle with the same diameter as the needle inner diameter (150 µm) is drawn for reference. Lines estimated cross-section area normalized to the needle cross-section area versus printing speed.

Figure 1f shows a cross-sectional scanning electron microscope (SEM) image of freeze-fractured lines printed at different speeds. From the estimated cross-section areas (see the Supporting Information), it can be seen that, at fixed extrusion pressure, the amount of material per unit of length is larger for the slower speeds. Consistently, with a constant volumetric flow rate of material through the needle tip, the product of the cross-section area times printing speed is constant for all the lines (Figure S2, Supporting Information). Printing speed also strongly influences the alignment of the deposited material (Figure S3, Supporting Information). The fact that thinned printed lines, with respect the needle inner diameter (ID), lead to clearly aligned birefringent lines highlights the relevance of the elongational flow mechanism, typically used to obtain aligned fibers of this type of materials.[25] Chain alignment occurs during shear flow in the needle, but especially also when the polymer is stretched between the receiving substrate and the needle tip.

2.2. Thermo-Actuation of 4D Printed LCE Elements with Uniaxial Orientation

Orientational order in crosslinked LCPs leads to anisotropy in mechanical properties and anisotropic thermal expansion.[26] In particular, LCEs exhibit large anisotropic deformation when changing their state of molecular order. A decrease of LC order induced by a temperature increase (Figure S4, Supporting Information) results in a contraction along the director and an expansion along its perpendicular direction (**Figure 2**a). This, together with the ability to locally define the LC director in the printed material using our methodology, allow to program material response to temperature. Single lines of material were printed on top of a thin-film of polyvinyl alcohol (PVA) previously deposited on glass. Once printed and fixed through photopolymerization, the resulting LCE lines are released from the substrate by immersing the sample in water that dissolves the PVA layer. Thermal contraction along the printing direction of these free-standing LCE lines is observed by hanging them from one extreme and heating them in an oven provided with an optical access (Figure 2b). LCE lines contract on heating from 30 to 90 °C to approximately half of their initial length. The samples relax back in seconds to nearly their original size by rapid cooling (Figure S5, Supporting Information), demonstrating immediate response of the LCE material to temperature opposite to that found in hydrogel swelling-based systems with notably slower response in the order of minutes.[9]

Continuous stripes of LCE with uniaxial orientation can be obtained by printing closely packed parallel lines along one direction. Printed lines fuse and lead to continuous films that keep the orientation imposed during the printing process (Figure S6, Supporting Information). Once cured and released from the substrate, heating of a free-standing stripe results in contraction along the line printing direction (long side of the stripe) and expansion along the perpendicular direction (Figure 2c). To explore the potential of the multilayer approach, a free-standing stripe consisting of eight printed layers of parallel lines has been prepared obtaining a 0.8 mm thick block of elastomer with monolithic uniaxial orientation. Upon heating from 30 to 90 °C, the stripe, that by itself weighs 0.17 g,

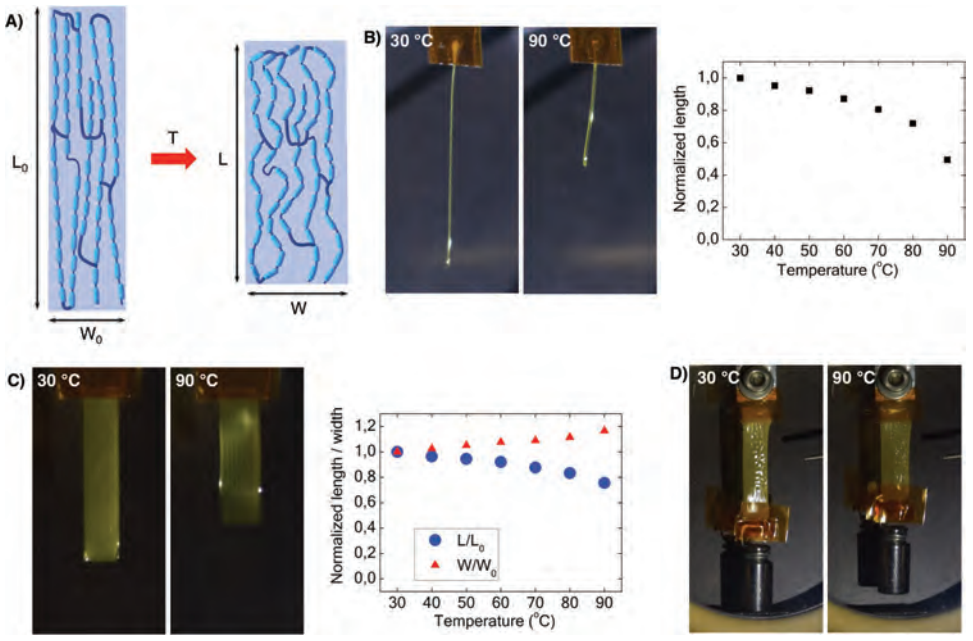

Figure 2. Thermoactuation of printed LCE elements with uniaxial orientation. a) Schematic representation of thermomechanical response of uniaxially aligned LCEs. Thermally induced mesogen disorder results in contraction along the director and expansion along the orthogonal direction. b) Thermomechanical deformation of a free-standing single LCE line. Normalized length versus temperature. c) Thermomechanical deformation of a free-standing rectangular stripe (15 × 3 mm). Normalized length and width versus temperature. d) Printed LCE multilayer (eight layers) stripe (25 × 6 mm). A weight of 5 g attached to the extreme of the stripe is lifted up on heating. Dimensions provided are those at RT. 2 mm s^{-1} deposition speed, needle ID: 330 µm.

contracts along the long direction lifting 5 g of weight over a length of 5 mm (Figure 2d), corresponding to a weight-specific work capacity of 1.44 J kg^{-1}, in the same range as homologous LCE systems.[21] Larger weights of 20 g have been raised with this stripe (Figure S7, Supporting Information). The additive character of our methodology holds the promise to generate predesigned large and thick structured elements with well-defined orientation at each position. They have high work capacity, overcoming in this way the limitation of small amount of actuation energy available in LCE thin-films, bringing these materials one step closer to real applications.

2.3. Thermo-Actuation of 4D Printed LCE Complex Elements

We have harnessed the opportunities offered by our 4D printing platform to prepare novel actuators with potential application in microfluidics, haptics, soft robotics, and adaptive optics.

Crosslinked LCP thin-films with complex director patterns varying in-plane have been demonstrated to be a powerful tool for shape-morphing flat membranes into 3D structures.[18–21] To demonstrate the potential of our printing technology, we produced a continuous layer with spiral-like director orientation. This orientation pattern was chosen as an approximation of an azimuthal pattern, having a continuous printing track (Figure S8, Supporting Information) that facilitates the formation of good-quality films through our platform. The sample (**Figure 3**a), with a slightly saddle-like form at 30 °C, relaxes to a stress-free, flat geometry at 45 °C. Progressive heating leads to a smooth change into a cone with its apex at the sample center as theoretically described by Warner and co-workers for azimuthal texture samples.[18] Multiple spirals printed together present the same thermoresponse, demonstrating the reproducibility of the technique and its potential to generate complex actuators over large areas (Figure 3b). The samples quickly revert in seconds to their original shape on fast cooling (Movies S1 and S2, Supporting Information). Properly integrated in devices through our printing platform, these cone-morphing membranes could potentially work as blisters for haptic displays or pumps in fluidic devices.

Moving forward from the current state of the art on thin-film processing, noncontinuous layers with open spaces can be easily prepared using our technology, creating new shape-morphing possibilities to this class of materials. Apertures in surfaces whose size and shape is addressed on demand can be used to prepare membranes able to filter different types and sizes of particles. As demonstrated by Modes et al., slits in a sheet of crosslinked LCP, surrounded by properly designed nematic textures, can open by changing their elongated shape into a rhomb on heating.[20] The texture consists of a piecewise constant −1 disclination defect bracketed with two piecewise constant +½ at the two ends of the slit. Tiling carefully, the plane with these slits leads to arrays of pores that activate upon external stimulus. Multiple aperture sheets can be easily obtained through our printing platform (Figure S9, Supporting Information) without the need for aggressively piercing a previously prepared patterned thin-film, as shown by Modes et al.[20] The 4D printed slits change size and shape by simply thermoactuating the film as shown in Figure 3c (Movie S3, Supporting Information). In another example of active porous sheets, we have printed an auxetic re-entrant honeycomb structure. Thermoactuation of this structure with the two extremes fixed on a frame (Figure 3d and Movie S4 (Supporting Information)) leads to large changes in pore shape, from re-entrant to conventional hexagonal honeycomb geometry, potentially useful in particle size and shape sorting devices.

Figure 3e shows a printed four-layer chiral structure fixed on a frame. The central circular ring is held by four LCE bands. The junctions of these bands with the circle are positioned at the four extremes of the white crosses depicted in the pictures. Heating induces the contraction of the bands holding the central ring that leads to its deformation from a circular shape into a square one. Concurrently, the junctions have changed their angular position, demonstrating rotation of the central annular object (Movie S5, Supporting Information). Beyond

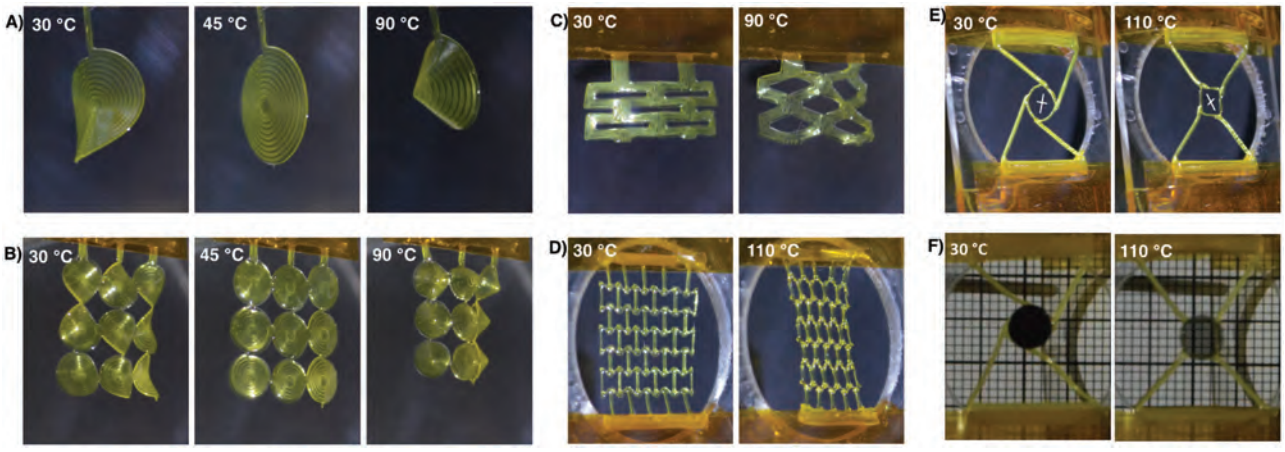

Figure 3. Thermoactuation of printed LCE complex elements. Free-standing films with a) spiral-like director texture (8 mm diameter) and b) nine spirals (5 mm diameter) printed together. c) Five slit sample in which each slit connects two pair of +½ discretized disclinations and cleaves a −1 disclination in two in the central part. d) Re-entrant honeycomb structure fixed at the two extremes (overall honeycomb structure dimensions: 12 × 12 mm). e) Framed four-layer chiral structure comprising a central ring (4.4 mm diameter) hold by four bands. f) The same chiral structure moves a round piece of linear polarizer on heating, therefore changing light transmission (a second polarizer is placed between the camera objective and the small round polarizer. Both polarizers are crossed at 30 °C). Dimensions provided are those at RT.

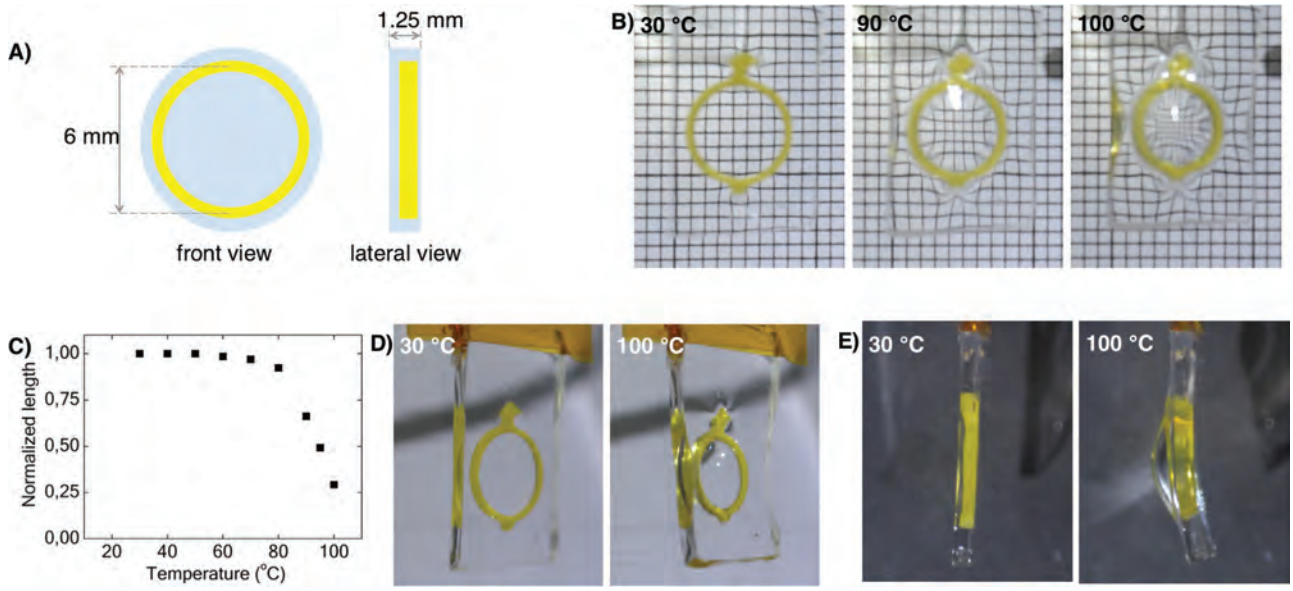

Figure 4. Integration of 4D printed LCEs with other materials. Adaptive optics. a) Schematic image of composite element consisting of a seven-layer LCE ring embedded in a PDMS slab. b) Grid observed though the LCE–PDMS element at different temperatures. The grid is 2.5 cm behind the element. c) Central square side length (normalized to the length at 30 °C) appears smaller as temperature increases. While the ensemble is flat at RT, bulging out of the PDMS toward the side far from the one of the LCE ring is observed at high temperature in an d) oblique and e) lateral view.

conventional objects translation, our technology allows to easily implement more sophisticated functions such as this rotation. This motion can, for example, be transferred to a round piece of linear polarizer as shown in Figure 3f, having potential applications in polarization monitoring, polarimetry, or temperature steered light transmission devices.

2.4. Integration of 4D Printed LCEs with Other Materials: Adaptive Optics

As an example of integration of the LCE elements with other materials, we have prepared a composite object consisting of a seven-layer ring of LCE embedded in a polydimethylsiloxane (PDMS) slab (**Figure 4**a). The possibilities of this LCE–PDMS ensemble as a variable focus lens have been explored. While the image of the grid placed 2.5 cm behind is nearly undeformed at RT, the size of the central squares is seen to largely diminish at high temperature, showing the lens character of our composite object (Figure 4b,c). To better understand the lens working principle, the ensemble has been closely observed (Figure 4d,e). At RT, the PDMS slab remains flat, however heating to 100 °C leads to a convex front of PDMS in one of the sides of the ensemble (concave in the other). Due to the fabrication method, the LCE ring is asymmetrically placed within the PDMS slab as schematically shown in Figure 4a (lateral view). This asymmetry together with stress introduced by the LCE ring upon heating leads to bulging out of the PDMS slab toward the side far from the LCE ring (Figure S10, Supporting Information). The deflection can be reversibly temperature-controlled and therefore the light wavefront curvature can also be modified, changing the focusing characteristics of the slab and demonstrating its potential as an adaptive optical element (Movie S6, Supporting Information).

3. Conclusions

In summary, we have introduced a 4D printing platform based on extrusion printing of LC polymeric materials for the preparation of responsive structures. The orientation conferred by the printing process advantageously leads to control over the orientation of the LC director of the deposited materials which is subsequently fixed by photopolymerization. This allows to precisely program magnitude and directionality of the strain and therefore 3D complex shape-morphing behavior of structures prepared using this technique. The additive character of this technology holds the promise to generate predesigned large-scale structured elements with well-defined orientation at each position. They can perform a large amount of work, narrowing the present gap between these materials and real applications. Complex morphing and functions, difficult to achieve with the currently available processing technologies, have been easily implemented using our 4D printing platform. This technology, that has been demonstrated for thermoresponsive elements, can be easily translated to photothermal response, making the system even more versatile and precise. Importantly, the actuation complexity may be enhanced by printing of other materials that are responsive to light, pH, magnetic or electric fields. Furthermore, the additive nature of the technology enables the manufacturing of unprecedented multimaterial–multiresponsive structures, performing sophisticated functions in robotics and optics, and on longer terms in (nano)medicine. Finally, integration of the presented structures with other materials, as demonstrated here with PDMS, could be easily extended to hydrogels that may lead to the formation of complex composite constructs of interest as platforms for mechanobiological studies. While revising this work, a paper disclosing the same basic 4D printing technology has been published by Ware and co-workers.[27]

4. Experimental Section

4.1. Materials

The mesogenic diacrylate 1,4-bis-[4-(6-acryloyloxyhexyloxy)benzoyloxy]-2-methylbenzene, usually referred as RM82 or C6M, was obtained from Merck. The chain extender *n*-butylamine was purchased from Aldrich. The UV photoinitiator 2-benzyl-2-(dimethylamino)-4′-morpholinobutyrophenone, also referred as Irgacure 369 was obtained from Aldrich. Tetrahydrofuran (THF) used as a solvent for the Michael addition reaction was purchased from Aldrich. Polyvinyl alcohol, 80% hydrolyzed, with M_w 9000–10 000 and used as a sacrificial layer for the release of the printed structures, was purchased from Aldrich.

4.2. Ink Preparation

Based on the synthetic procedure reported by Ware et al.[21] the amine and the reactive monomer were added to a flask in a 1:1.01 molar ratio. 1 wt% photoinitiator was added to the mixture. THF, the same weight as the total reactants content, was added as solvent for the reaction. The solution is homogenized using a magnetic stirrer and allowed to react for 24 h at 70 °C in an open flask. After 24 h, the sample recovered the initial weight, prior to THF addition, within 1 wt%.

4.3. Printing Equipment

The printer was built on the basis of a modified CNC router chassis. The machine tool, usually mounted in this router above the flatbed, could move in the *XYZ* axes, therefore allowing the tool to sculpt the object that is placed in a fixed position below. The machine tool was substituted in this printing setup by an ink reservoir provided with an extrusion needle, all embedded in a temperature-controlled metallic block that stabilized the temperature of the ink. The reservoir was pressurized when printing was carried out. With these modifications, the printing head could describe *X*, *Y*, *Z* motions and extrude at the same time material on demand. The tip was positioned at the supporting substrate. This point served as reference for the CNC router. Printing was controlled by WinPC-NC. Computer-aided design (CAD) files were generated using Libre-Cad freeware software. G-code commands were initially generated by using CAD fusion software from Aerotech Inc. Modifications of the code for a correct interface with the modified CNC router were done using a home-made software.

4.4. 3D Printing of LCE Structures

The ink consisted of the linear main chain polymer that resulted from the Michael addition reaction and the photoinitiator. This mixture was charged in a UV protected barrel for printing. The linear material was extruded through a tip (30 and 23 gauge with inner diameters of 150 and 330 µm, respectively). A 30 gauge tip was employed in samples shown in Figure 1, while 23 gauge was used for all the samples for thermoactuation experiments. The barrel was heated to 70 °C, while the receiving substrate was kept at RT to help printed line stabilization. Printing was carried out on conventional glass microscope slides, except for those samples to be released (shape-morphing samples) that were printed on top of a 150 nm PVA layer. Prior to printing, glass slides were cleaned with isopropanol in an ultrasound bath for 10 min and subsequently dried before use. Printing of structures was carried out using the 3D printer described above. The separation of the printing tip and the substrate was maintained constant during printing of each layer at a typical height of tens to hundreds of micrometers. Deposition speeds were in the range of 0.5–4 mm s^{-1} (2 mm s^{-1} unless specified). Following printing of a layer, the deposited structures were exposed to a UV fluorescent lamp (365 nm, 3 mW cm^{-2}) for 2 min. in order to fix the molecular orientation. Printing of successive layers was done in the same way but raising the printing head a fixed height for each successive layer (typical height step used: 100–140 µm). After finishing the printing of the last layer, the sample was exposed at RT to UV light from an EXFO lamp (365 nm, 10 mW cm^{-2}) for 5 min each of the sides of the printed sample.

4.5. LCE–PDMS Adaptive Lens Preparation

The composite optical systems comprising a LCE ring and a layer of PDMS were fabricated as follows. A multilayer ring of LCE (6 mm diameter at 30 °C) was printed and cured on a PVA layer as described above. The released ring was placed on top of a flat cyclic olefin polymer (COP) microscope slide. PDMS elastomer was prepared from Sylgard-184 (Dow Corning). The silicone base and curing agent in a 98:2 ratio were thoroughly mixed using a spatula. To eliminate bubbles, the uncured mixture was degassed by putting it in a vacuum desiccator at 100 mbar for 30 min. The PDMS precursor mixture was poured on top of the LCE ring and a second layer of COP was placed on top in a plano-parallel fashion. To fix the thickness of the PDMS layer, two slides (1.25 mm thick) were used as spacers between the COP layers. The PDMS was cured for 24 h at 50 °C. The LCE–PDMS ensemble was then released from the COP layers at RT.

4.6. Polarization Optical Microscopy

The LC structures were examined under a POM (Nikon Eclipse 80I), coupled to a hot-stage (Linkam LTSE420).

4.7. Characterization of the Structure Morphology

SEM was performed on JEOL (JSM-IT100) at 10 kV under high vacuum, after coating the sample with a 25 nm gold layer. The cross-section was obtained by fracturing the sample in liquid nitrogen.

4.8. Thermoactuation Characterization

For morphing experiments, free-standing samples were prepared. To obtain them, printing was carried out on PVA coated glass substrates. These were prepared by applying a 5 wt% solution in milliQ water by spin coating at1800 rpm for 60 s and then dried at 60 °C for 10 min. After printing and curing, the structures were released from the substrate by immersing them in water. After few hours, the structure was released and could be carefully picked with a piece of paper, dried, and fixed to a Kapton tape in one extreme. Thermal actuation and shape recovery experiments of the free-standing samples were carried out in a home-made aluminum oven cavity provided with a glass cover that allowed deformation observation. The samples were hanged inside the aluminum cavity and temperature was monitored using a thermocouple placed close to the sample. Actuation was monitored using two digital cameras Nikon D3300 and D5200.

Supporting Information

Supporting Information is available from the Wiley Online Library or from the author.

Acknowledgements

C.S.-S. thanks the Spanish MINECO project SAF2014-54763-C2-2-R, the Gobierno de Aragón, and the FEDER (EU). D.J.B. thanks the European Research Commission (ERC) Advanced Grant 66999 (VIBRATE). D.L. thanks the Netherlands Organization of Scientific Research (NWO) VENI grant 15135. The authors thank Sergio Galve for help with the G-Code programming, Chris van Heesch for conceptual illustrations, and Scott Mitchell for stimulating discussions.

Conflict of Interest

The authors declare no conflict of interest.

Keywords

3D printing, actuators, adaptive optics, liquid crystalline polymers, soft robotics

Received: October 18, 2017
Revised: October 22, 2017
Published online: December 6, 2017

[1] E. T. Roche, R. Wohlfarth, J. T. B. Overvelde, N. V. Vasilyev, F. A. Pigula, D. J. Mooney, K. Bertoldi, C. J. Walsh, *Adv. Mater.* **2013**, *26*, 1200.
[2] B. Zhou, W. Xu, A. A. Syed, Y. Chau, L. Chen, B. Chew, O. Yassine, X. Wu, Y. Gao, J. Zhang, X. Xiao, J. Kosel, X.-X. Zhang, Z. Yao, W. Wen, *Lab Chip* **2015**, *15*, 2125.
[3] Y. M. Song, Y. Xie, V. Malyarchuk, J. Xiao, I. Jung, K.-J. Choi, Z. Liu, H. Park, C. Lu, R.-H. Kim, R. Li, K. B. Crozier, Y. Huang, J. A. Rogers, *Nature* **2013**, *497*, 95.
[4] N. Torras, K. E. Zinoviev, J. Esteve, A. Sánchez-Ferrer, *J. Mater. Chem. C* **2013**, *1*, 5183.
[5] D. Rus, M. T. Tolley, *Nature* **2015**, *521*, 467.
[6] R. F. Shepherd, F. Ilievski, W. Choi, S. a. Morin, A. a. Stokes, A. D. Mazzeo, X. Chen, M. Wang, G. M. Whitesides, *Proc. Natl. Acad. Sci. USA* **2011**, *108*, 20400.
[7] P. Martins, A. C. Lopes, S. Lanceros-Mendez, *Prog. Polym. Sci.* **2014**, *39*, 683.
[8] J. Kim, J. A. Hanna, M. Byun, C. D. Santangelo, R. C. Hayward, *Science* **2012**, *335*, 1201.
[9] A. Sydney Gladman, E. A. Matsumoto, R. G. Nuzzo, L. Mahadevan, J. A. Lewis, *Nat. Mater.* **2016**, *15*, 413.
[10] T. Ikeda, J.-I. Mamiya, Y. Yu, *Angew. Chem., Int. Ed.* **2007**, *46*, 506.
[11] T. J. White, D. J. Broer, *Nat. Mater.* **2015**, *14*, 1087.
[12] A. Agrawal, T. Yun, S. L. Pesek, W. G. Chapman, R. Verduzco, *Soft Matter* **2014**, *10*, 1411.
[13] Y. L. Yu, M. Nakano, T. Ikeda, *Nature* **2003**, *425*, 145.
[14] G. N. Mol, K. D. Harris, C. W. M. Bastiaansen, D. J. Broer, *Adv. Funct. Mater.* **2005**, *15*, 1155.
[15] S. Iamsaard, S. J. Aßhoff, B. Matt, T. Kudernac, J. J. L. M. Cornelissen, S. P. Fletcher, N. Katsonis, *Nat. Chem.* **2014**, *6*, 229.
[16] M. Yamada, M. Kondo, J.-I. Mamiya, Y. Yu, M. Kinoshita, C. J. Barrett, T. Ikeda, *Angew. Chem., Int. Ed.* **2008**, *47*, 4986.
[17] A. H. Gelebart, D. J. Mulder, M. Varga, A. Konya, G. Vantomme, E. W. Meijer, R. L. B. Selinger, D. J. Broer, *Nature* **2017**, *546*, 632.
[18] C. D. Modes, K. Bhattacharya, M. Warner, *Phys. Rev. E* **2010**, *81*, 060701.
[19] L. T. de Haan, C. Sánchez-Somolinos, C. M. W. Bastiaansen, A. P. H. J. Schenning, D. J. Broer, *Angew. Chem., Int. Ed.* **2012**, *51*, 12469.
[20] C. D. Modes, M. Warner, C. Sánchez-Somolinos, L. T. de Haan, D. Broer, *Proc. R. Soc. A* **2013**, *469*, 20120631.
[21] T. H. Ware, M. E. McConney, J. J. Wie, V. P. Tondiglia, *Science* **2015**, *347*, 982.
[22] C. L. van Oosten, C. W. M. Bastiaansen, D. J. Broer, *Nat. Mater.* **2009**, *8*, 677.
[23] R. L. Truby, J. A. Lewis, *Nature* **2016**, *540*, 371.
[24] T. H. Ware, T. J. White, *Polym. Chem.* **2015**, *6*, 4835.
[25] A. H. Gelebart, M. Mc Bride, A. P. H. J. Schenning, C. N. Bowman, D. J. Broer, *Adv. Funct. Mater.* **2016**, *26*, 5322.
[26] D. J. Broer, G. N. Mol, *Polym. Eng. Sci.* **1991**, *31*, 625.
[27] C. Ambulo, J. J. Burroughs, J. M. Boothby, H. Kim, M. R. Shankar, T. H. Ware, *ACS Appl. Mater. Interfaces* **2017**, *9*, 37332.